Comparing the Performance of Vertical and Diagonal Piles Group at the Normal Fault Rupture

Mohammad Davoodi[1], Mohammad Kazem Jafari[2], Fatemeh Ahmadi[3]*

1. Assistant Professor, Geotechnical Engineering Department, International Institute of Earthquake Engineering and Seismology (IIEES), Iran,
* Corresponding Author; email: m-davood@iiees.ac.ir
2. Professor, Geotechnical Engineering Department, International Institute of Earthquake Engineering and Seismology (IIEES), Iran
3. M.Sc. Student, International Institute of Earthquake Engineering and Seismology (IIEES), Iran

ABSTRACT

The applied loads on structures caused by fault rupture can be divided into vertical and lateral loads. There is a common agreement between researchers that diagonal piles would perform better than vertical piles under lateral loads. However, an area of uncertainty still remains: Would the diagonal piles still perform better under various load combinations? The 1999 Kocaeli earthquake was an appropriate case for monitoring the performance of vertical piles. In this paper, based on the evidence provided by Kocaeli earthquake, a study has been done to compare the vertical and diagonal piles behavior. This study is conducted in two analysis steps. First, surface fault rupture is propagated through soil in the free-field. Second, the models of the piles group is subjected to a differential displacement the same as Step 1. Totally, it can be concluded that the acceptable performance of diagonal piles group occurs only when the fault emerges near the left center of cap. Otherwise, the vertical piles group would perform better.

1. Introduction

Surface fault rupture is a phenomenon that happens due to the relative displacement of the ground on the both sides of the fault at the time of earthquake. Reviewing the history of the intensive earthquakes shows that some considerable and irreparable damages have incurred to different important structures and industrial installations by the surface fault rupture.

The destructive recent Turkey and Taiwan earthquakes and their dangerous surface fault ruptures necessitated developing progress in the designing methods and instructions against the fault rupture. Most of the numerical [1-4] and laboratory [5-7] analysis have been focused on the verification of the fault rupture on the shallow foundations and just a few numerical analysis have been performed on deep foundations.

Anastasopoulos [8, 9] developed a two-step finite element methodology to study the propagation of a fault rupture through soil and its interplay with the foundation-structure system. The centrifuge-validated methodology was applied to study the Kocaeli case histories one by one. The results indicated that the presence of a structure on top of an outcropping fault may have a significant influence on the rupture path. The heavy structures founded on continuous and rigid foundations, the fault rupture diverts substantially and may avoid rupturing underneath

the structure. It was also found that the structures in the vicinity of faults can be designed to survive significant dislocations.

In the past, some methods have been applied to design soil-structure systems to sustain large tectonic deformation. These methods were studied by Anastasopoulos et al on the buildings of a housing complex, a 400 m viaduct bridge, some highway bridges, a cut-and-cover tunnel, a lane-cover tunnel and a deep immersed tunnel [10-12]. Fadaee [13] suggested a thick diaphragm-type of soil bentonite wall (SBW) to protect a structure founded on a rigid raft. The SBW was installed in front of and near the foundation at sufficient depth to intercept the propagating fault rupture.

Anastasopoulos [3] presented a methodology for design of bridges against tectonic deformation. Fixed-head piled foundations are shown to be rather vulnerable to faulting-induced deformation. Floating piles perform better than end-bearing piles, and if combined with hinged pile-to-cap connections, they could survive much larger offsets.

Loli [14] presented a combined experimental and numerical study of normal fault rupture-caisson interaction. It is found that the rigid caisson body acts as a kinematic constraint, always forcing the fault rupture to divert or bifurcate around the structure.

Anastasopoulos [15] investigated the interplay of surface fault rupture with an embedded two by four pile foundation, as it propagates in a moderately dense sand stratum. It was shown that even for a moderate fault offset, lightly reinforced piles would fail structurally, while also forcing the pile cap and the bridge pier on top to undergo substantial rotation and displacement. Even heavy reinforcement might not prevent potentially disastrous displacements.

The basic goal of this paper is to verify the fault rupture propagating and to compare the performance of diagonal piles group with vertical piles group at the fault rupture by 3D finite element modeling.

2. Constitutive Model

Experimental and numerical studies have shown that post-peak soil behavior is a decisive factor in fault rupture propagation and its possible emergence on the ground surface [16]. The behavioral model utilized in fault rupture modeling is the Mohr-Coulomb with strain softening. As shown in Figure

(1), strain softening defined as decreasing the friction angle φ_{mob} and dilation angle Y_{mob} versus increasing plastic shear strain. For $o \le \gamma_{oct}^p < \gamma_f^p$ these parameters can be introduced by:

$$\left[\begin{array}{l} \varphi_{mob} = \varphi_p - \dfrac{\varphi_p - \varphi_{res}}{\gamma_f^p} \gamma_{oct}^p \\[4mm] Y_{mob} = Y_p \left(1 - \dfrac{\gamma_{oct}^p}{\gamma_f^p} \right) \end{array} \right] \qquad (1)$$

where φ_p is an ultimate friction angle, φ_{res} is the residual value of the friction angle, Y_p is the ultimate dilation angle, γ_f^p is the plastic shear strain at the end of softening, and γ_{oct}^p is the octahedra plastic shear strain. For $\gamma_{oct}^p \ge \gamma_f^p$, the residual value of friction angle and dilation angle has been used.
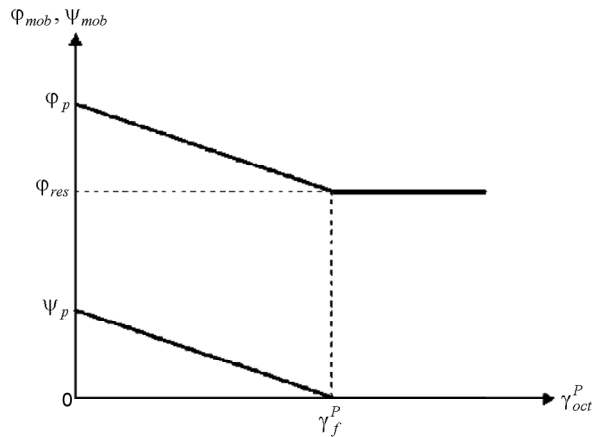

Figure 1. Variation of the friction angle φ_{mob} and dilation angle Ψ_{mob} versus plastic shear strain [12].

The variation of stress ratio and volume changes versus horizontal displacement of the soil has been shown in Figure (2). From this figure, it can be seen that the soil before reaching yield (OA) deforms quasi elastically. In this region, a little nonlinear deformation with no dilatation can be observed. Between the points *A* and *B*, the soil yields and enters into the plastic region, expands and reaches to the peak point of *B*. σx_p is defined as horizontal displacement for $\tau/\sigma_v = \max$. In the *BC* zone, the soil experiences softening, and on the right side of the peak, a horizontal shear strip develops at the middle of the soil sample height. The softening is completed at the point *C*. is defined as the horizontal displacement for $-\delta y/\delta x = 0$. At the end, the shear propagates along the shear strip in CD zone.
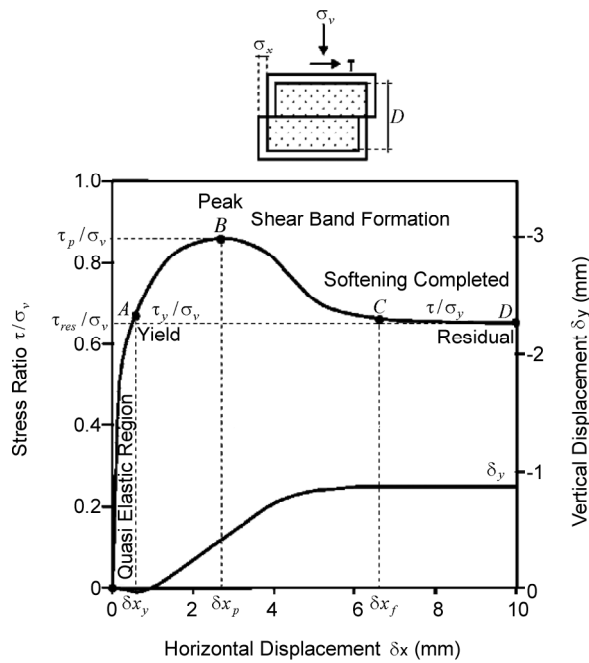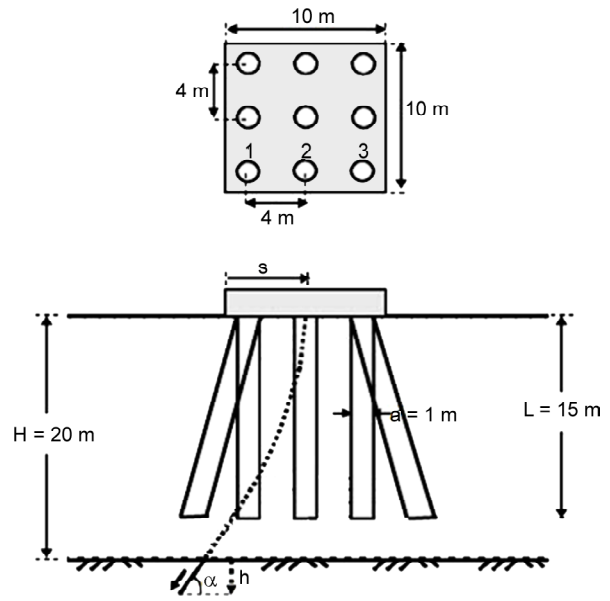
Figure 2. Variation of stress ratio and volume changes versus horizontal displacement in the direct shear test [12].

Figure 3. Piles group in the path of a rupturing fault, d = 1m, L = 15 m.

In the case that the sample is in the region after *B* (at the right side of the peak), the shear strip has been made. Shibuya et al [17] assumed that the entire plastic shear deformation occurs along the strip shear while the rest of the soil remains elastic. Assuming shear strip width (d_B) equals to $16d_{50}$ where d_{50} is the mean size of the sand grains, the plastic shear strain where the softening is completed defined as below:

$$\gamma_f^p = \gamma_p^p + \frac{\delta x_f - \delta x_p}{16d_{50}} = \frac{\delta x_p - \delta x_y}{D} + \frac{\delta x_f - \delta x_p}{16d_{50}} \quad (2)$$

3. Analysis Methodology

Figure (3) shows the geometry and dimensions of piles group. It is considered a uniform soil deposit of thickness *H* at the base of which a normal fault, with angle of dip α, produces downward displacement of vertical amplitude *h*. The analysis is conducted in two steps. First, fault rupture propagation through soil is analyzed in the free-field, ignoring the presence of the structure. Then, a capped piles group foundation placed on top of the free-field fault outcrop at a specified distance *S* (measured from the left side of the pile cap), and the analysis of deformation of the soil-structure system due to the same base dislocation *h* is performed. In order to highlight the interaction

between a piled foundation and an emerging fault rupture, two typical foundation systems are examined:

1) a 3×3 capped vertical piles group,
2) a 3×3 capped diagonal piles group.

As shown in Figure (3), the piles length (L_p) is 15 m with 1 m diameter (d_p) that spaced 4 m apart from center to center. The piles in system 2 are divided into two groups, the piles in hanging wall and footwall are diagonal with dip angle 10° (measured from vertical), and piles in middle row are vertical. Their cap is 10 m × 10 m in plan, 2.5 m thick, and carries a structural vertical load of 10 MN [18]. A rigid connection is assumed between the cap and piles (fixed-head piles). The piles modeled with linear elastic beam elements.

A three-dimensional (3D) finite-element (FE) model, using eight-nodded elements, was developed for this research. The model was created and analyzed using a general finite-element software, ABAQUS 6-11.

In both cases, the soil deposit consisted of dense sand, of total thickness *H* = 20 m, normal fault imposed with α = 60°. Idealized soil materials are utilized in the analysis: $\varphi_p = 45°$, $Y_p = 15°$, $\varphi_{res} = 32°$, $\gamma_f^p = 0.05$ [18]. The optimum element size of the model in the free field condition has been selected and compared with experimental results. The selected element size was then used in the final finite element model. The elements of soil and pile have tied

together.

The relative location of outcropping is varied parametrically through the distance *S*. Three positions of the piles group with respect to the outcropping fault in the free field are examined: *S* = 2, 4 and 8 m.

4. Result

4.1. Fault Rupture Propagation in the Free-Field

To confirm the results of numerical modeling in free field condition, the data of the centrifuge test conducted at the University of Dundee [16] has been used. In the centrifuge test, normal fault with the angle of $\alpha = 60°$ has been applied to the compacted dry soil ($Dr = 80\%$). The parameters and the dimension of the soil in centrifuge test are shown in Table (1) and Figure (4). The parameters used for numerical modeling are: $\varphi_p = 39°$, $Y_p = 11°$, $\varphi_{res} = 30°$, $\gamma_f^p = 0.215$.

Table 1. Summary of basic parameters and prototype dimensions of centrifuge experiments [12].

| Fault Type	g (m/s²)	Dr (%)	H (m)	L (m)	W (m)	H (max)
Normal	100	80	25	68	20	1.91
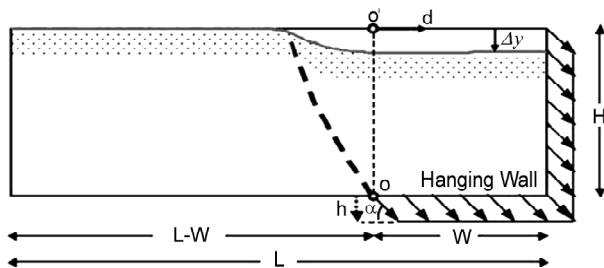
Figure 4. The model dimensions and the centrifuge test definitions (normal fault) [12].

The deformed mesh of numerical analysis and laboratory test can be shown in Figure (5). Besides, the vertical deformation of the ground surface for both cases can be shown in Figure (6). The small variance in applied deformations (*h*) for finite element analysis (*h* = 1) and for the centrifuge test (*h* = 1.08) can be acceptable. Nevertheless, there are some differences between the analysis and laboratory test results. This difference can be related to the second rupture line induced in experiment (at the right side of the main fault in Figure (5b)), which was not predicted by the analysis.
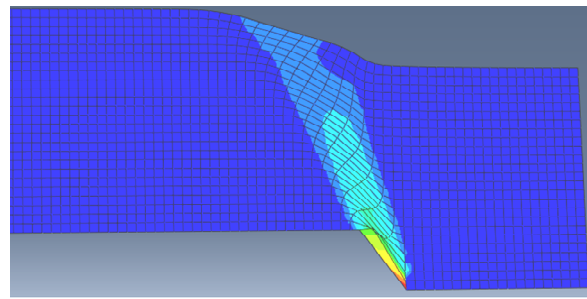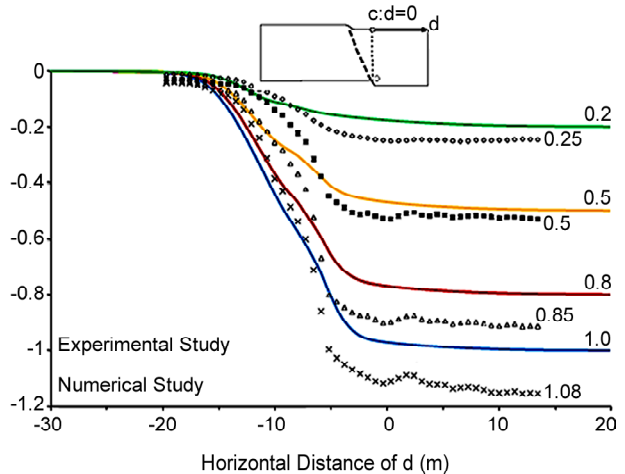

Numerical Analysis
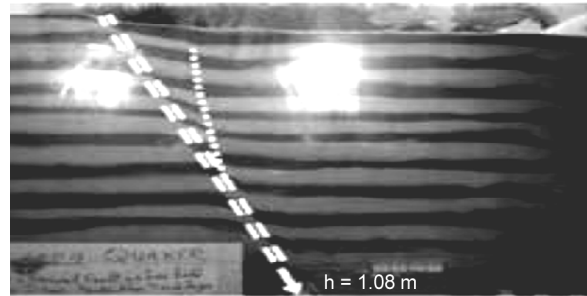
Laboratory Test [12]

Figure 5. Comparison between the numerical deformed mesh and photograph from centrifuge test.

Figure 6. Comparing the vertical deformation of the ground surface for numerical and experimental study.

4.2. Fault Rupture with Soil- Pile Interaction

After the confirmation of the numerical modeling results in the free field condition, the deformation analysis of the soil-structure system due to the same base dislocation was performed. Based on the analysis results, the distribution of plastic strains, lateral displacement of cap, distortion angle (β) of ground, the largest bending moment in the piles for a parametrically variable ratio of base dislocation over layer thickness (*h/H* = 1-5%) has been evaluated.

4.2.1. Deformation Response

The deformed mesh of piles group and the distribution of plastic strains in 3D model can be shown in Figure (7). Figures (8) and (9) portray the comparison between analysis results of vertical and diagonal piles for each S values (S = 2, 4, 8 m). In all cases, the vertical pile results are compared with diagonal pile results to visualize the effects of dip angle of pile.

Figure (8) shows the lateral displacement of

(a) Vertical

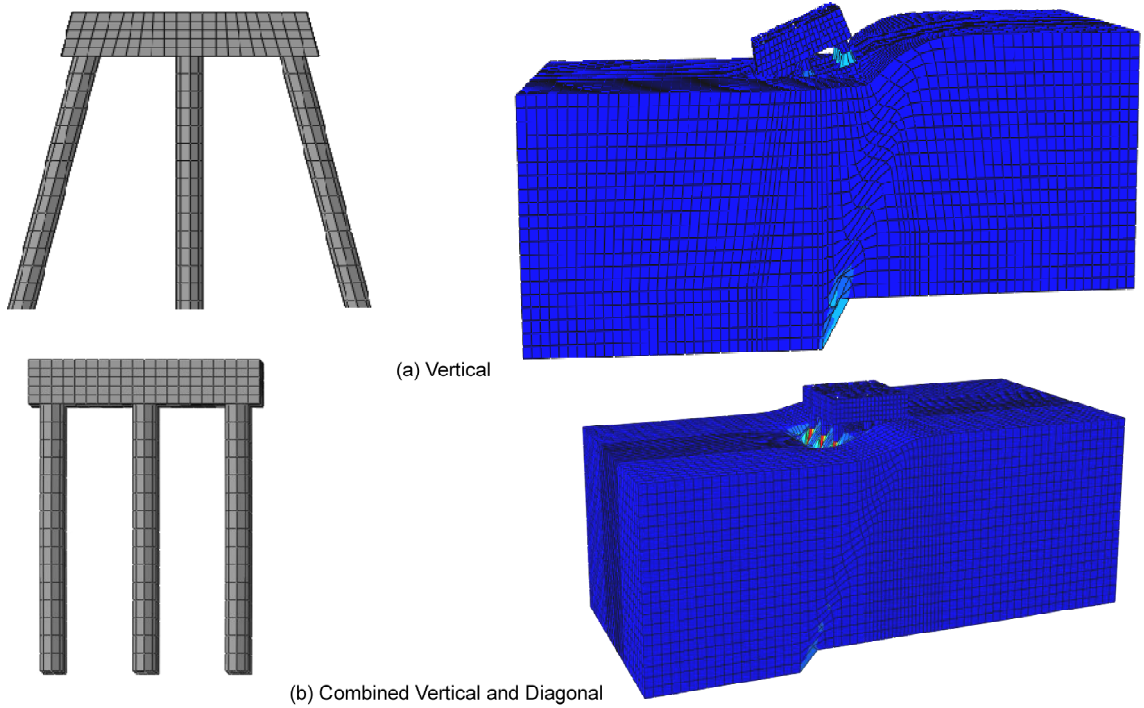(b) Combined Vertical and Diagonal

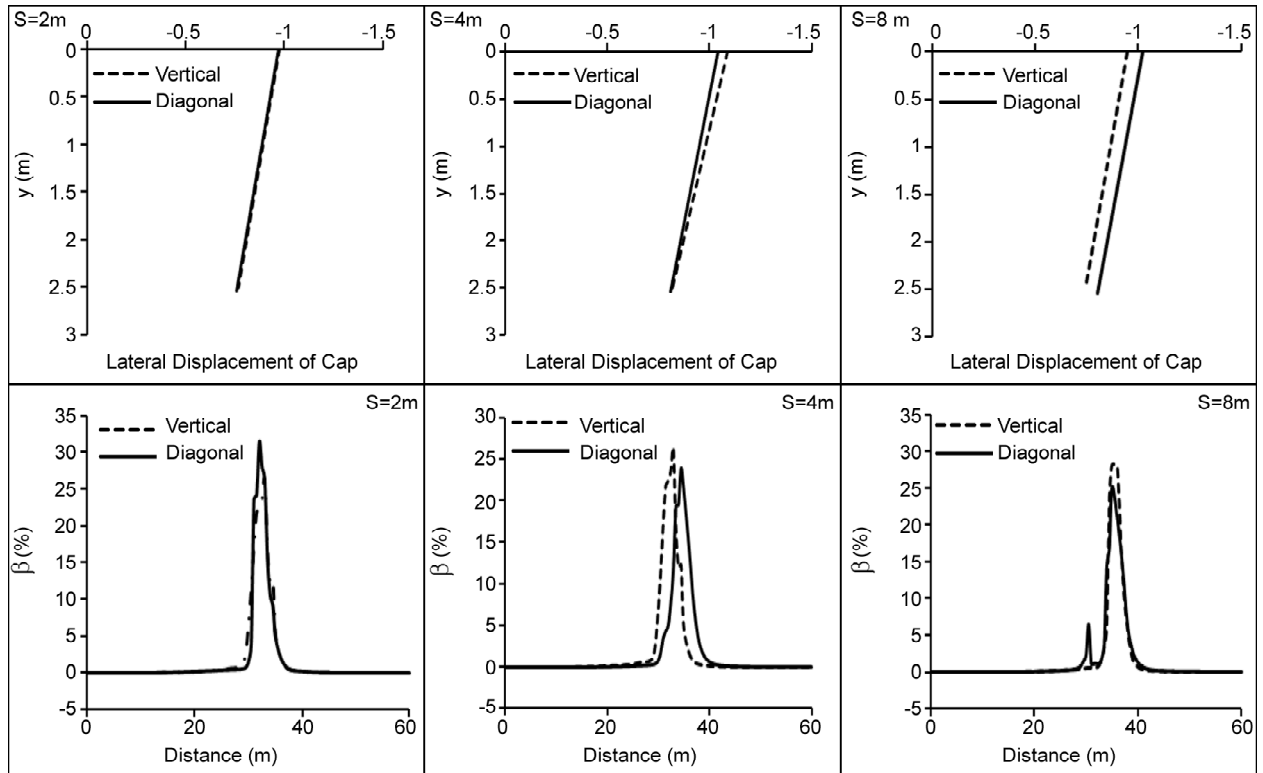**Figure 7.** Deformed mesh for the piles group (left side) and 3D FEM (right side) at the fault rupture.

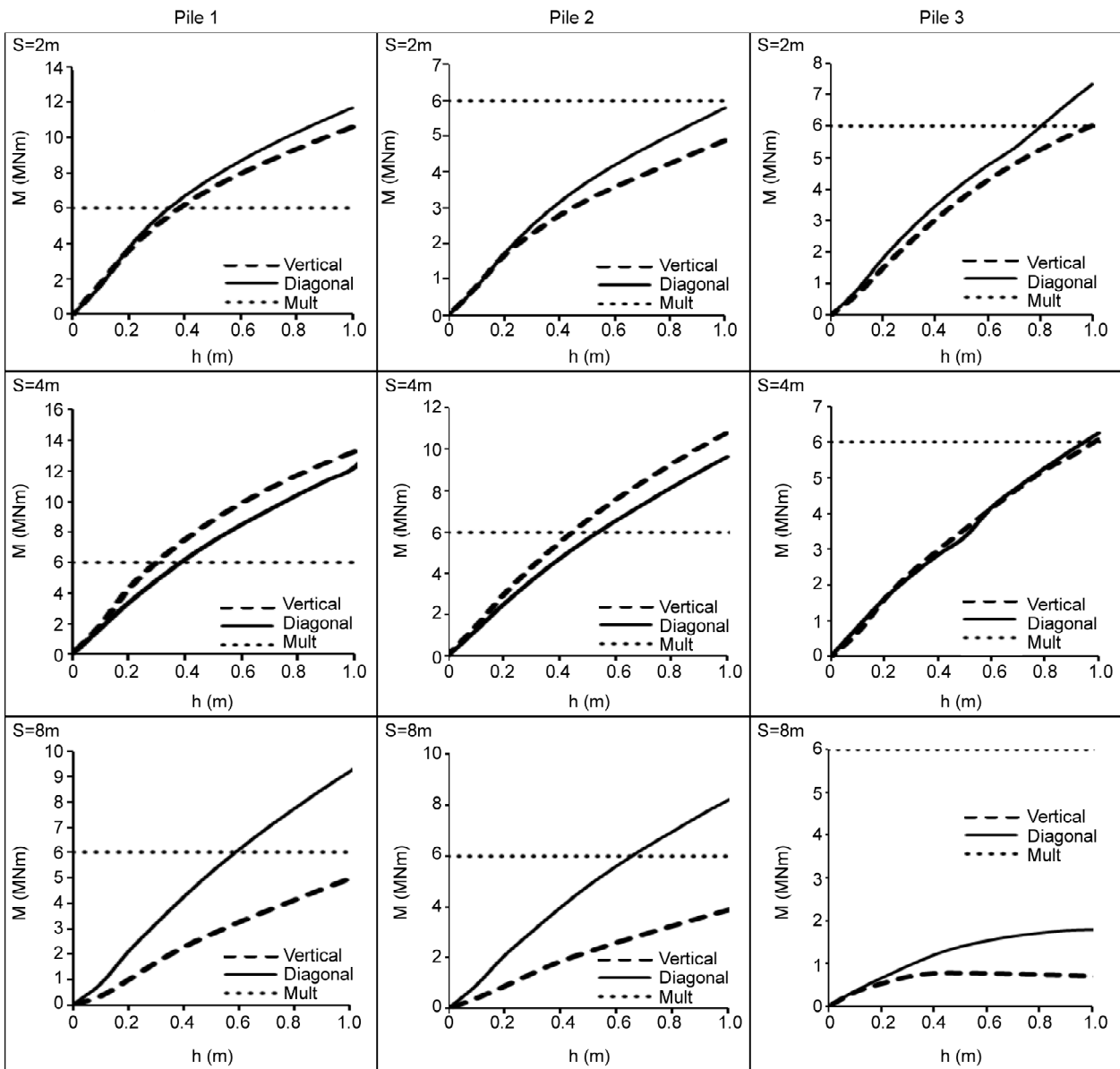**Figure 8.** Lateral displacement of cap, distortion angle β, for the largest base dislocation h = 1 m.

Figure 9. Largest bending moment in the piles.

cap and the distortion angle (β) of ground for each S value. For $S = 2$ m, when the fault emerges near the left edge of the piles group and the group is therefore almost all in the footwall, in both cases the rupture path hits the piles group. As a result, in system 1, rupture path diverts to the right about 6 m, and in system 2 about 5 m towards the footwall. Therefore, diversion of the rupture path is about 20% higher in system 1. This magnitude is about 30% higher in system 2, for $S = 4$ m. There is no considerable difference between displacement or rotation of the vertical and diagonal pile's cap for $S = 2$ m and $S = 4$ m. When the fault emerges near the right edge of the piles group ($S = 8$ m), diversion of the rupture path is about 25% higher in the

vertical pile. Displacement or rotation of the diagonal pile's cap is about 30% higher than that in vertical pile's cap.

4.2.2. Moment Response

Shown in Figure (9) are the largest bending moment in the piles 1, 2 and 3. For $S = 2$ m, Pile 1 (completely in hanging wall) is being pulled outward and downward by dropping the hanging wall of the fault.

As a result, very large bending moments would develop at the pilehead, in excess of 10 MNm in system 1 and 11 MNm in system 2 for a dislocation of 1 m. Therefore, this magnitude is about 10% higher in the system 2.

Piles 2 and 3 (almost in footwall) would experience much less distress. In pile 2, maximum bending moment would occur at the top, in excess of 4 MNm in system 1 and 5 MNm in system 2. In pile 3, maximum bending moment would occur at 8 m depth, in excess of 6 MNm in system 1 and 7 MNm in system 2 for a dislocation of 1 m. In both piles, this magnitude is about 25% higher in the system 2.

Naturally, such large bending moments would exceed the ultimate capacity (Mu) of the $d = 1$ m piles. In fact, the ultimate design capacity is used for comparing the performance of piles before reaching failure and is described with moment-curvature relationships. Such relationships are obtained using standard cross-sectional analysis for reinforced concrete.

With a very heavy reinforcement ratio on the order of 4%, Mu was calculated as 6 MNm. This means that, the hanging wall side piles (i.e. pile 1) would be the first to fail, at h = 0.38 m in system 1 and at $h = 0.34$ m in system 2. The following failure would occur in footwall side piles (i.e. pile 3), at $h = 0.95$ m in system 1; and at $h = 0.8$ m in system 2. Finally, the medium row (i.e. pile 2) would fail at $h > 1$ m, in system 1 and system 2.

For $S = 4$ m, large bending moments would exceed the ultimate capacity; the hanging wall side piles (i.e. pile 1) would be the first to fail, at $h = 0.3$ m in system 1 and at $h = 0.38$ m in system 2. The following failure would occur in footwall side piles (i.e. pile 3), at $h = 0.44$ m in system 1; and at $h = 0.55$ m in system 2. The medium row piles (i.e. pile 2) would fail at $h = 0.94$ m in system 1; and at $h > 1$ m in system 2.

Finally, for $S = 8$ m, the hanging wall side piles (i.e. pile 1) would be the first to fail, at $h > 1$ m in system 1 and at $h = 0.58$ m in system 2. The following failure would occur in medium side piles (i.e. pile 2), at $h > 1$ m in system 1; and at $h = 0.66$ m in system 2. Finally, the footwall side row (i.e. pile 3) would fail at $h > 1$ m in system 1 and system 2.

5. Conclusions

This paper has presented the results of a numerical study on normal surface fault rupture-piles group interaction. Two typical foundation systems including diagonal piles (system 1) and diagonal-

vertical piles (system 2) were modeled. The key findings obtained through numerical examinations have been summarized as follows:

The angle between rupture and piles would become different from initial angle of fault rupture. When the fault emerges near the left center of the cap ($S < 5$ m), the angle between rupture and pile would be less than initial imposed angle in system 2. Therefore, the transferred vertical component of the force to the pile is less than that in system 1. In this case that the piles group is almost all in the footwall, piles sustain larger imposed deformation before reaching failure in system 2. For both systems at $S = 4$ m, the rupture path hits the piles group and diverts to the right. However, diversion of the rupture is higher in system 2.

In contrast, when $S > 5$ m for the recalled systems, the angle between rupture and piles is more than initial angle in system 2. The vertical component of the force that is transferred to the piles is more than that in system 1. Therefore, piles in system 2 sustain smaller imposed deformation before reaching failure. Besides, diversion of the rupture path is smaller in system 2.

Based on the evidence of this paper, it can be concluded that when $S < 5$ m, diagonal piles would have better performance than vertical piles. In contrast, when $S > 5$ m, the vertical piles would act more satisfactory.

References

1. Yilmaz, M. T. and Paolucci, R. (2007) Earthquake fault rupture-shallow foundation interaction in undrained soils. *Earthquake Engineering and Structural Dynamics*, **36**(1), 101-118.

2. Paolucci, R. and Yilmaz, M.T. (2008) Simplified theoretical approaches to earthquake fault rupture-shallow foundation interaction. *Bulletin of Earthquake Engineering*, **6**(4), 629-644.

3. Anastasopoulos, I., Gazetas, G., Drosos, V., Georgarakos, T., and Kourkoulis, R. (2008a) Design of bridges against large tectonic deformation. *Earthquake Engineering and Engineering Vibration*, **7**(4), 345- 368.

4. Anastasopoulos, I., Gazetas, G., Bransby, M.F., Davies, M.C.R., and El Nahas, A. (2009) Normal fault rupture interaction with strip foundations.

Journal of Geotechnical and Geoenvironmental Engineering, ASCE, **135**(3), 359-370.

5. Bransby, M.F., Davies, M.C.R., El Nahas, A., and Nagaoka, S. (2008a) Centrifuge modeling of normal fault-foundation interaction. *Bulletin of Earthquake Engineering*, **6**(4), 585-605.

6. Bransby, M.F., Davies, M.C.R., El Nahas, A., and Nagaoka, S. (2008b) Centrifuge modeling of reverse fault-foundation interaction. *Bulletin of Earthquake Engineering*, 6(4), 607-628.

7. Ahmed, W. and Bransby, M.F. (2009) The interaction of shallow foundations with reverse faults. *Journal of Geotechnical and Geoenvironmental Engineering*, **135**(7), 914-924.

8. Anastasopoulos, I. and Gazetas, G. (2007a) Foundation-structure systems over a rupturing normal fault: Part I. Observations after the Kocaeli 1999 earthquake. *Bulletin of Earthquake Engineering*, **5**(3), 253-275.

9. Anastasopoulos, I. and Gazetas, G. (2007b) Behavior of structure- foundation systems over a rupturing normal fault: Part II. Analysis of the Kocaeli case histories. *Bulletin of Earthquake Engineering*, **5**(3), 277-301

10. Anastasopoulos I. and Gazetas G. (2005) Design against fault rupture: methodology and applications in Greece. *Proceedings of the 1ˢᵗ Greece - Japan Workshop: Seismic Design, Observation and Retrofit of Foundations, Athens*, 345-366.

11. Anastasopoulos I., Antonakos G., and Gazetas G. (2010) Slab foundations subjected to thrust faulting: parametric analysis and simplified design method. *Soil Dynamics and Earthquake Engineering*, **30**(10): 912-924.

12. Anastasopoulos, I., Gerolymos, N., Drossos, V., Kourkoulis, R., Georgarakos, P., and Gazetas, G. (2008b) Behavior of deep immersed tunnel under combined major fault rupture and strong seismic shaking. *Bulletin of Earthquake Engineering*, **6**(2), 213-239.

13. Fadaee, M., Anastasopoulos, I., Antonakos, G., Gazetas, G., Jafari, M.K., and Kamalian, M. (2013) Soil bentonite wall protects foundation from trust faulting: analyses and experiment. *Earthquake Engineering and Engineering Vibration*, **12**(3), 473-486.

14. Loli, M., Bransby, M.F., Anastasopoulos, I., and Gazetas, G. (2011) Interaction of caisson foundations with a seismically rupturing normal fault: centrifuge testing versus numerical simulation. *Geotechnique*, **62**(1), 29-43

15. Anastasopoulos, I., Kourkoulis, R., Gazetas, G., and Tsatsis, A. (2013) Interaction of piled foundation with a rupturing normal fault. *Geotechnique*, **63**(12), 1042-1059.

16. Anastasopoulos, I., Gazetas, G., Bransby, M.F., Davies, M.C.R., and El Nahas A. (2007a) Fault rupture propagation through sand: finite element analysis and validation through centrifuge experiments. *Journal of Geotechnical and Geoenvironmental Engineering*, ASCE, **133**(6), in press

17. Shibuya, S., Mitachi, T., and Tamate, S. (1997) Interpretation of direct shear box testing of sands as quasisimple shear. *Geotechnique*, **47**(4), 769-790.

18. Gazetas, G., Anastasopoulos, I., and Apostolou, M. (2007) 'Shallow and deep foundations under fault rupture or strong seismic shaking'. In: *Earthquake Geotechnical Engineering*, Pitilakis, K.D. (Ed.), Springer, Netherlands, 185-215.